

**Cross-plane Seebeck coefficient and Lorenz number in superlattices**

Z. Bian, M. Zebarjadi, R. Singh, Y. Ezzahri, and A. Shakouri

*Electrical Engineering Department, University of California, Santa Cruz, California 95064, USA*

G. Zeng, J-H. Bahk, and J. E. Bowers

*Department of Electrical and Computer Engineering, University of California, Santa Barbara, California 93106, USA*

J. M. O. Zide and A. C. Gossard

*Materials Department, University of California, Santa Barbara, California 93106, USA*

(Received 9 July 2007; published 9 November 2007)

Low dimensional and nanostructured materials have shown great potential to achieve much higher thermoelectric figure of merits than their bulk counterparts. Here, we study the thermoelectric properties of superlattices in the cross-plane direction using the Boltzmann transport equation and taking into account multiple minibands. Poisson equation is solved self-consistently to include the effect of charge transfer and band bending in the potential profile. The model is verified with the experimental data of cross-plane Seebeck coefficient for a superlattice structure with different doping concentrations. The simulations show that thermoelectric properties of superlattices are quite different from those of bulk materials because the electronic band structure is modified by the periodic potential. The Lorenz numbers of superlattices are surprisingly large at low carrier concentrations and deviate far away from the Wiedemann-Franz law for bulk materials. Under some conditions, the Lorenz number could be reduced by 50% compared to the bulk value. Most significantly, the Seebeck coefficient and the Lorenz number of superlattices do not change monotonically with doping concentration. An oscillatory behavior is observed. The effects of temperature and well and barrier thicknesses on the cross-plane Seebeck coefficient and Lorenz number are also investigated.

DOI: [10.1103/PhysRevB.76.205311](https://doi.org/10.1103/PhysRevB.76.205311)

PACS number(s): 73.50.Lw, 73.21.Cd

**I. INTRODUCTION**

Thermoelectric materials have attracting applications in solid-state refrigeration and direct thermal-to-electrical energy conversion. However, their use is still limited mainly due to the poor efficiency. The efficiency can be simply measured by the dimensionless thermoelectric figure of merit  $ZT = S^2 \sigma T / K$ , where  $S$  is the Seebeck coefficient,  $\sigma$  is the electrical conductivity,  $K$  is the thermal conductivity, and  $T$  is the absolute temperature. The difficulty in finding a good thermoelectric material lies in the interdependence of electrical conductivity, Seebeck coefficient, and thermal conductivity. There has been renewed interest in thermoelectric materials since it has been proved theoretically and experimentally that thermoelectric figure of merit of a given material system can be greatly improved by using low dimensional and nanometer-scale structures. In the cross-plane direction of heterostructure multilayers and multiple quantum well superlattices, the thermoelectric power factor can be increased by using thermionic emission and filtering of high energy electrons.<sup>1-6</sup> Another benefit of such materials is the reduction of thermal conductivity, which has been observed experimentally<sup>7-9</sup> and explained theoretically by the enhanced phonon scattering by heterointerfaces and nanoparticles.<sup>10-14</sup>

The thermoelectric charge transport in multiple quantum well superlattices in the cross-plane direction has been investigated extensively based on the thermionic emission theory.<sup>15</sup> However, there is an inherent difficulty in keeping the continuity of both electrical current and Peltier heat flux in this model. Besides, local density of states of an average bulk medium were used which is suitable only when the

mean free path of charge carriers is less than one superlattice period and the coherence is lost from inelastic scattering.<sup>16</sup> On the other hand, in order to utilize the thermal conductivity minima of superlattice materials, the superlattice period should be around 10 nm or less, which is usually less than the mean free path of electrons. Only a few papers have used the density of states of superlattices, but the very first lower minibands were considered in the calculations.<sup>16,17</sup> This is not enough for thermoelectric transport because the optimal position of the Fermi energy is within  $\sim k_B T$  from the barrier band edge and many higher minibands should be also included especially for tall barrier and highly doped superlattices. In a recent paper, multiple minibands were concluded; however, since only two periods of superlattices were used, the miniband dispersion relation could not be constructed and eventually the variation of group velocity for different states was ignored.<sup>18</sup> Furthermore, a fixed barrier height was assumed in the above literatures, although the band edge profile and miniband structure change with temperature and doping concentration due to the charge redistribution in space. Due to the incomplete modeling, the electronic thermal conductivities of superlattices were usually estimated roughly according to the Wiedemann-Franz law of bulk materials.<sup>9</sup> In this paper, we will solve the coupled Schrödinger and Poisson equations self-consistently and calculate the dispersion relation for each miniband. When multiple minibands are included in electrothermal transport calculations, we find different behaviors of Seebeck coefficient and Lorenz number compared to bulk materials when the temperature changes. The cross-plane Lorenz number of superlattices is surprisingly high at low carrier concentrations, which distinguishes itself from the Wiedemann-Franz law of

bulk materials. The oscillatory behavior of the Seebeck coefficient and the Lorenz number as functions of doping concentration and factors, which are affecting the oscillations, are discussed.

## II. MODELING

We calculated the electronic band structure of superlattices using the envelope-function method and the Kronig-Penney model in one-dimensional crystal.<sup>19,20</sup> One superlattice period  $d$  is segmented into small size elements. In each element, the potential is assumed to be constant and the wave function solution of the Schrödinger equation can be written as

$$E_i < V(z): \quad \psi_i(z) = A_i \exp(\beta_i z) + B_i \exp(-\beta_i z),$$

$$E_i > V(z): \quad \psi_i(z) = A_i \sin(\alpha_i z) + B_i \cos(-\alpha_i z), \quad (1)$$

where  $V(z)$  is the potential and  $E_i$  is the eigenenergy of electron in the cross-plane direction. For parabolic band, the wave numbers are

$$\beta_i^2 = \frac{2m^*}{\hbar^2} [V(z) - E_i], \quad \alpha_i^2 = \frac{2m^*}{\hbar^2} [E_i - V(z)]. \quad (2)$$

If the kinetic energy  $E_k = E_i - V(z)$  is much larger than zero, the nonparabolicity of band dispersion can be included by replacing the effective mass in Eq. (2) with  $m^*(1 + \alpha E_k)$ , where  $\alpha$  is the nonparabolicity factor. The wave functions in adjacent elements are connected at the interface by the continuity of wave functions and currents. According to Bloch's theorem for periodic structures, wave functions at the start and at the end of one period are different only by a phase coefficient

$$\psi_i(z + d) = \psi_i(z) \exp(iq_n d), \quad (3)$$

where  $q_n$  is the Bloch wave vector satisfying the periodic boundary condition for  $N$  periods of the superlattices:

$$q_n N d = n \times 2\pi, \quad (4)$$

where  $n$  is an integer. For each quantized  $q_n$  in the first Brillouin zone, the electron energy  $E$  along the cross-plane direction is varied to find the eigenenergy  $E_i$  and eigenfunction  $\psi_i$  in each miniband  $i$  which satisfy Eqs. (1)–(3). Now, we revise the indices of energy and wave functions to reflect the miniband level and the Bloch wave vector. The Fermi energy and charge distribution are found through charge neutrality equation, i.e., the total surface doping density in the  $x$ - $y$  plane is equal to the integral of the charge distribution along the  $z$  direction, which is described by

$$n(z) = \frac{m^*}{\pi \hbar^2} \sum_n \sum_i |\psi_{ni}(z)|^2 \int_0^\infty f_0(E_{\parallel} + E_{ni}) (1 + 2\alpha E_{\parallel}) dE_{\parallel}, \quad (5)$$

where  $E_{\parallel}$  is the kinetic energy in the plane and  $f_0$  is the Fermi-Dirac distribution. For parabolic band ( $\alpha=0$ ), the integral in the plane has an analytical solution and the charge distribution is reduced to

$$n(z) = \sum_n \sum_i \frac{m^* k_B T}{\pi \hbar^2} \ln \left[ 1 + \exp\left(\frac{E_f - E_{ni}}{k_B T}\right) \right] |\psi_{ni}(z)|^2. \quad (6)$$

Subsequently, the band bending can be calculated from the Poisson equation using above charge distribution:

$$\frac{d}{dz} \left( \epsilon(z) \frac{d}{dz} \right) \phi(z) = -e [n(z) - N_d^+(z)], \quad (7)$$

where  $e$  is the electron charge, and  $N_d^+(z)$  is the concentration of ionized dopant. Here, for  $n$  type materials, the contribution of holes is neglected. The band bending is then used to update the total potential profile

$$V(z) = e\phi(z) + \Delta E_c(z), \quad (8)$$

where  $\Delta E_c$  is the conduction band offset. The new potential profile changes the solution of the miniband structure according to Eqs. (1)–(3). Thus, iterations are performed until both the potential and miniband structures converge. After solving the miniband structures, the group velocity of each eigenstate along the cross-plane direction can be calculated from the dispersion curves:

$$v_{ni} = \frac{1}{\hbar} \frac{\partial E_{ni}}{\partial q_n} \quad (9)$$

The electrical conductivity  $\sigma$ , the Seebeck coefficient  $S$ , and the electron contribution to thermal conductivity  $K_e$  of bulk semiconductor materials can be derived from the Boltzmann transport equation with the relaxation time approximation. They are all integral functions of the differential conductivity<sup>21</sup>

$$\sigma_d(E) = e^2 \tau(E) v_z^2(E) \rho(E) \left( -\frac{\partial f_0(E)}{\partial E} \right), \quad (10)$$

where  $\tau$  is the electron momentum relaxation time and  $\rho$  is the density of states of conduction band. By decoupling the density of states of in-plane and cross-plane directions, the above equation can be modified to the one applicable to anisotropic superlattices:

$$\sigma_{ni}(E_{\parallel}) = e^2 \frac{m^*}{\pi \hbar^2} (1 + 2\alpha E_{\parallel}) \tau(E_{\parallel} + E_{ni}) v_{ni}^2(E_{ni}) \times \left( -\frac{\partial f_0(E_{\parallel} + E_{ni})}{\partial (E_{\parallel} + E_{ni})} \right). \quad (11)$$

The contributions of all the electron states to  $\sigma$ ,  $S$ , and  $K_e$  are counted by continuous integrals in the in-plane direction and summations of discrete states of multiple minibands in the cross-plane direction:

$$\sigma = \sum_n \sum_i \int_0^\infty \sigma_{ni} dE_{\parallel}, \quad (12)$$

$$S = \frac{1}{eT} \frac{\sum_n \sum_i \int_0^\infty (E_{\parallel} + E_{ni} - E_f) \sigma_{ni} dE_{\parallel}}{\sum_n \sum_i \int_0^\infty \sigma_{ni} dE_{\parallel}}, \quad (13)$$

$$K_e = \frac{1}{eT^2} \left[ \frac{\sum_n \sum_i \int_0^\infty (E_{\parallel} + E_{ni})^2 \sigma_{ni} dE_{\parallel}}{\left[ \sum_n \sum_i \int_0^\infty (E_{\parallel} + E_{ni}) \sigma_{ni} dE_{\parallel} \right]^2} - \frac{\sum_n \sum_i \int_0^\infty \sigma_{ni} dE_{\parallel}}{\sum_n \sum_i \int_0^\infty \sigma_{ni} dE_{\parallel}} \right]. \quad (14)$$

For *n*-type materials, the Seebeck coefficient is usually with a negative sign because the electron charge is negative and the average energy of electrons contributing to charge transport is larger than the Fermi energy. The sign of Seebeck coefficient might change when the Fermi level moves across subminibands of low dimensional materials due to the oscillation of density of states. In the following calculations, we do not see any positive sign of Seebeck coefficient because the quantum confinement and energy quantization are only in the cross-plane direction. For convenience, the term ‘‘Seebeck coefficient’’ denotes its amplitude in the following text and its sign is taken as negative by default. According to the Wiedemann-Franz law, the ratio of electronic thermal conductivity to electrical conductivity of a metal is the product of the temperature and a constant  $\pi^2/3(k_B/e)^2$  called ‘‘Lorenz number.’’ The unitless Lorenz number can be defined as

$$L = \left( \frac{e}{k_B} \right)^2 \frac{K_e}{T\sigma}, \quad (15)$$

which is reduced to  $\pi^2/3$  for metal. Similarly, the unitless Lorenz number can be calculated from Boltzmann transport and electronic band structures of semiconductor materials. It can be shown that for bulk semiconductors, the unitless Lorenz number  $L$  depends on the major mechanism of electron (or hole) scattering and changes slightly around 3 with the carrier density when polar optical phonon scattering and impurity scattering dominate.<sup>21</sup> The unitless Lorenz number will be investigated in the following section.

### III. RESULTS

InGaAs/InGaAlAs superlattices lattice matched to InP substrate and embedded with ErAs semimetallic nanoparticles were grown with the molecular beam epitaxy method. This is a flexible material system because the well-barrier conduction band offset can be adjusted by changing the relative composition of Ga and Al in the barrier. When the Ga:Al ratio is 60%:40%, the conduction band offset is about 0.2 eV. The measurements showed increased Seebeck coefficient and reduced thermal conductivity.<sup>5,6,9</sup> In the previous work, there were noticeable discrepancy between modeling and experiment and the electron contribution to the total thermal conductivity was estimated according to the Wiedemann-Franz law of bulk materials. In the following, we focus on the calculation of thermoelectric properties based firmly on multiple miniband transport. For simplicity and in order to study mainly the effect of superlattice mini-

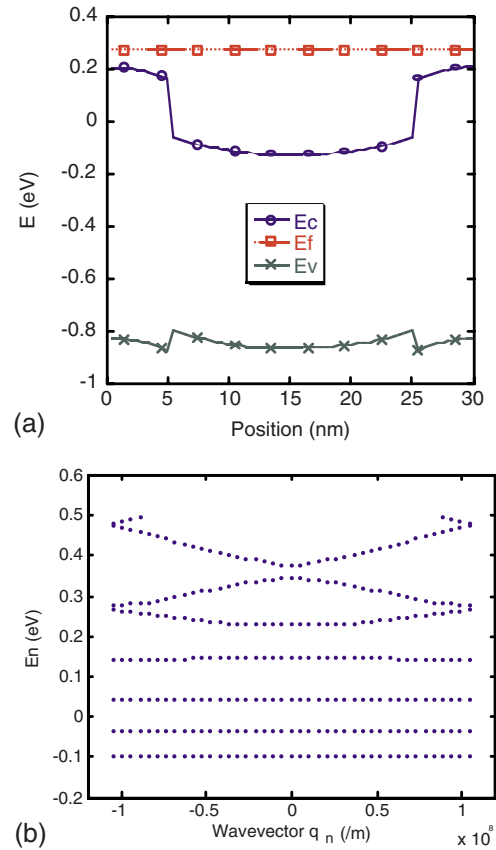


FIG. 1. (Color online) (a) The band profile of one superlattice period. (b) The dispersion curves of minibands.

bands, we will not include the electron scattering of ErAs nanoparticles. The InGaAs wells are assumed doped uniformly while the InGaAlAs barriers are not doped. When there is no external electrical field and temperature gradient, the Fermi level tends to be the same everywhere at equilibrium. Thus, there is charge transfer from well regions (with higher Fermi level than barrier regions before charge transfer) to barrier regions and the resulting built-in field modifies the band profile. The band profile affects the quantized levels and dispersion curves of minibands. This also modifies how these minibands are filled with electrons and changes the Fermi level and the charge redistribution in space. So a self-consistent calculation is needed for the simulation of the miniband structure and the Fermi level. It is interesting to note that besides doping concentration, the temperature change also affects the band profile for a given superlattice structure. The band profile and miniband structures calculated from a self-consistent solution of the coupled Schrödinger and Poisson equations are shown in Fig. 1 for superlattices with well width 20 nm, barrier width 10 nm, and conduction band offset 0.2 eV. The temperature is 300 K and the well regions are *n*-type doped with a total electron concentration  $10^{19} \text{ cm}^{-3}$ . It can be seen that the effective barrier height becomes larger due to the charge transfer from the wells to the barriers. The amplitude of group velocity is larger for a higher miniband, indicating the electron energy filtering which is consistent with the thermionic emission model.<sup>15</sup>

At room temperature and above, polar optical phonon scattering and ionized impurity scattering are the two major electron scattering mechanisms in InGaAs and InGaAlAs alloys. The electron momentum relaxation time due to polar phonon scattering is<sup>22</sup>

$$\frac{1}{\tau_p} = \frac{e^2 \omega_0 (\kappa_0 / \kappa_\infty - 1)}{4 \pi \kappa_0 \epsilon_0 \hbar \sqrt{2E/m^*}} \left[ N_0 \sqrt{1 + \frac{\hbar \omega_0}{E}} + (N_0 + 1) \sqrt{1 - \frac{\hbar \omega_0}{E}} - \frac{\hbar \omega_0 N_0}{E} \sinh^{-1} \left( \frac{E}{\hbar \omega_0} \right)^{1/2} + \frac{\hbar \omega_0 (N_0 + 1)}{E} \sinh^{-1} \left( \frac{E}{\hbar \omega_0} - 1 \right)^{1/2} \right], \quad (16)$$

where  $\omega_0$  is the angular frequency of the optical phonon,  $\kappa_0$  and  $\kappa_\infty$  are the static and high frequency dielectric constants, and  $N_0$  is the number of optical phonons given by Bose-Einstein statistics:

$$N_0 = \frac{1}{\exp(\hbar \omega_0 / k_B T) - 1}. \quad (17)$$

The electron momentum relaxation time due to ionized impurity scattering is<sup>22</sup>

$$\tau_i = \frac{16 \sqrt{2m^*} \pi \kappa_\infty^2 \epsilon_0^2}{N_1 e^4} \left[ \ln(1 + \gamma^2) - \frac{\gamma^2}{1 + \gamma^2} \right]^{-1} E^{3/2}, \quad (18)$$

where  $N_1$  is the concentration of ionized impurities, and  $\gamma^2 \equiv 8m^* E L_D^2 / \hbar^2$ . The Debye screening length  $L_D$  is  $(\kappa_\infty \epsilon_0 k_B T / e^2 n)^{1/2}$  for nondegenerate semiconductors, and  $(2\kappa_\infty \epsilon_0 E_f / 3e^2 n)^{1/2}$  for degenerate semiconductors, where  $n$  is the charge carrier concentration. The electron momentum relaxation time used in Eq. (11) can be calculated by  $\tau = (1/\tau_p + 1/\tau_i)^{-1}$ .

With the changes of barrier width and Al composition in barriers, the scattering rate should be changed accordingly for an accurate calculation. Approximately, the electron momentum relaxation time of bulk InGaAs (with  $\kappa_0 = 13.9$ ,  $\kappa_\infty = 11.6$ , and  $\hbar \omega_0 = 34$  meV) are used in the subsequent calculations of thermoelectric transport coefficients. First, we calculate the Seebeck coefficient and the Lorenz number of the superlattices structure described above as functions of doping concentration in the well regions. In Fig. 2, we compare the results for two cases: fixed barrier height (0.2 eV) and self-consistent solutions. The comparison of these two cases has two purposes: one is to verify the self-consistent calculation, and the other is to study the effects of charge transfer and band bending. It can be seen in Fig. 2(a) that the Seebeck coefficient for the case of self-consistent solution is larger than that for a fixed barrier height. This can be explained by the charge transfer and band bending and the resulting increase of the effective barrier height for electron energy filtering. It is also interesting to see in Fig. 2(b) that although there is some slight difference in unitless Lorenz number for the fixed barrier and self-consistent solutions of superlattices, they have the same trend with the change of carrier concentration. Surprisingly, we find that the Lorenz

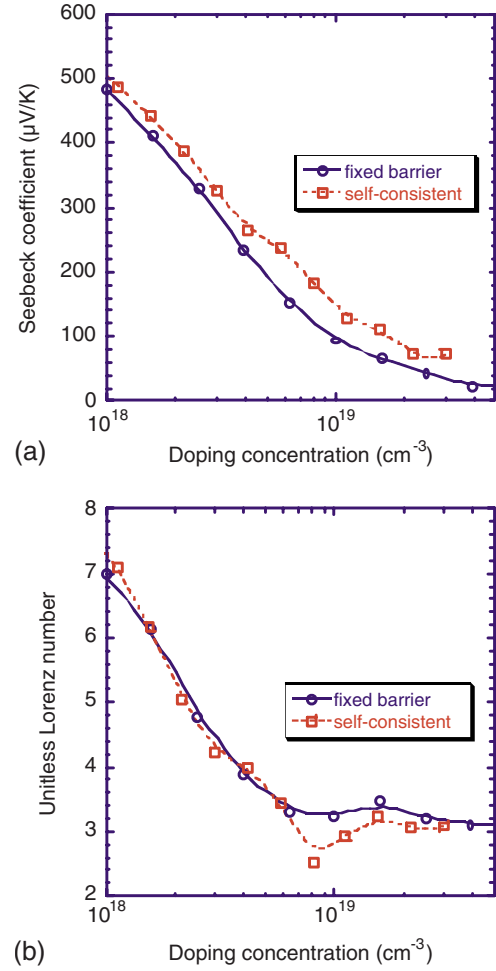


FIG. 2. (Color online) (a) The Seebeck coefficients and (b) the Lorenz numbers for the case of fixed barrier height (0.2 eV) and the case of self-consistent solutions including band bending.

number can be much larger than 3 at low doping concentrations, which is clearly different from bulk materials and cannot be predicted intuitively.

It is difficult to verify the modeling with experiments because it is very challenging to measure the thermoelectric properties of thin films in the cross-plane direction very accurately. The current or temperature uniformity and thermal leakage are big issues for thermoelectric measurements of thin films due to their high aspect ratios of device area to film thickness. Parasitic effects such as electrical and thermal contact resistances are typically annoying in extracting intrinsic properties of the thermoelectric thin film because their amplitudes and their variations from device to device are not negligible. To measure the cross-plane Seebeck coefficient of InGaAs/InGaAlAs superlattices, mesa structures were formed using conventional microelectronics processing techniques and microheaters were integrated on the top of the devices to create the temperature difference in the cross-plane direction. The details of the device structures were described in the Fig. 1 of Ref. 6. We measured the Seebeck coefficient of superlattice materials using two different methods. One is at University of California Santa Barbara (SB) in which the temperature is measured at steady state by a mi-

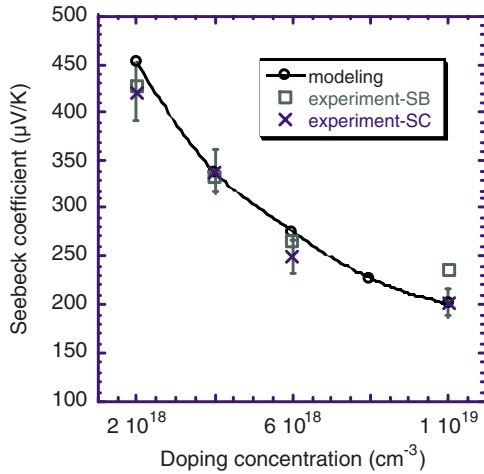


FIG. 3. (Color online) The comparison of the modeling and experimental data of the cross-plane Seebeck coefficient for InGaAs/InGaAlAs superlattices.

crothermocouple and the Seebeck coefficient of superlattices is extracted using the calibrated property of InP substrate and the finite element thermal analysis of the temperature distribution across multiple layers.<sup>6</sup> The second measurement is done at University of California Santa Cruz (SC) using the  $3\omega$  method. A sinusoidal current at frequency  $\omega$  is sent to the heater, the Seebeck voltage across the active semiconductor materials is measured at  $2\omega$ , and the temperature across the whole structure is calculated from the ratio of  $3\omega$  to  $1\omega$  components of the heater voltage. A separate calibration is done to extract the temperature dependence of the heater resistance. The same electrical power is applied to the heater on the top of a reference device with the same geometry but without the thin film layer. Then the net temperature and Seebeck voltage across the top thin film layer can be extracted from the total by deducting the substrate and other parasitic contributions using the measurement data of reference device. So there is no need of modeling of temperature drop across the electrical insulation layer and thermal interface. Then the Seebeck coefficient of superlattices is calculated from the ratio of the net Seebeck voltage to the net temperature drop across the thin film. In Fig. 3, the measured Seebeck coefficients using the two methods described above are plotted together with the modeling. Compared to the plot in Fig. 2(a) for the case of self-consistent solution, nonparabolic band dispersion is added here in the modeling for a more accurate analysis. It can be seen that they agree with each other very well even without any fitting parameters in the modeling. The slight discrepancy between modeling and experiments at low carrier concentrations might be due to neglecting ErAs particle scattering of electrons, which is comparable to impurity scattering at low doping concentrations.

Now, we assume the conduction band is parabolic in the following discussions and focus on how the superlattice period and the potential profile can modify the thermoelectric transport. We expect that the temperature dependence of the thermoelectric properties of superlattices can be different from bulk materials because of the relative alignment of

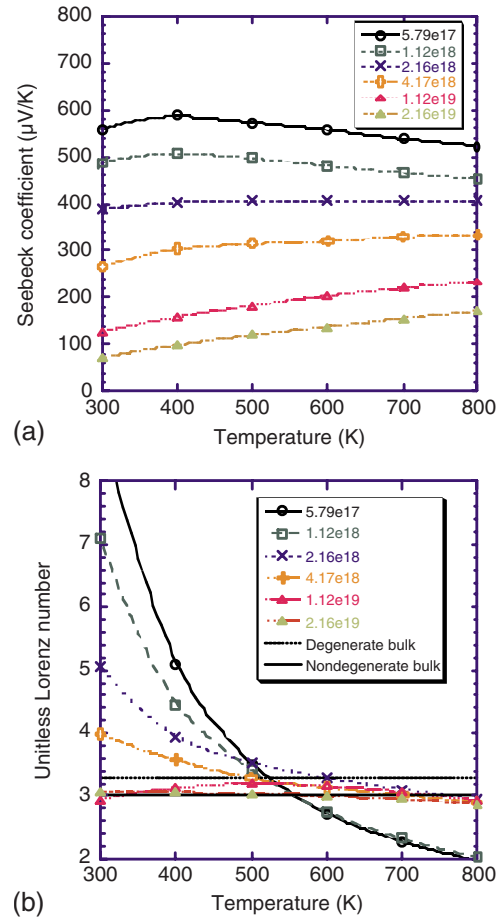


FIG. 4. (Color online) The temperature dependences of (a) the Seebeck coefficient and (b) the Lorenz number of superlattices in the cross-plane direction.

minibands, Fermi energy, and potential barriers. This is demonstrated in Fig. 4, where the temperature dependences of Seebeck coefficients and Lorenz numbers are plotted for different doping concentrations for the above superlattices structure. The Seebeck coefficient for the two small doping concentrations increases first and decreases later when the temperature increases. One should note that increase in temperature has two effects on electron transport: one is the broadening of Fermi window  $-\partial f_0/\partial E$ , and the other is the increase of Fermi energy. The former can explain the increase of Seebeck coefficient with temperature. The latter is responsible for the decrease of Seebeck coefficient with temperature at low carrier concentrations and high temperatures regime where the Seebeck coefficient is sensitive to the position of Fermi energy. It can also be seen that compared to the constant values of the Lorenz numbers of degenerate and nondegenerate bulk semiconductors, the Lorenz number of superlattices changes quite a lot with temperature. The Lorenz numbers are surprisingly large for low doping concentrations at low temperatures, in which the Fermi energy is deep in the wells. These observations indicate a significant deviation from the Wiedemann-Franz law in cross-plane direction of superlattices.

For bulk materials, the product of the three terms  $v_z^2(E)\rho(E)(-\partial f_0(E)/\partial E)$  making up the differential conduc-

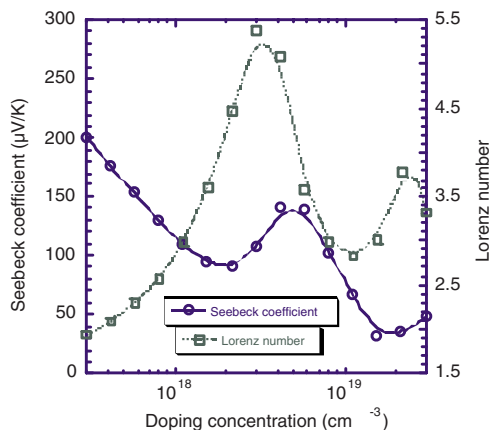


FIG. 5. (Color online) The Seebeck coefficient and the unitless Lorenz number of a short period superlattice structure (well 6 nm, barrier 3 nm, at 300 K).

tivity [see Eq. (10)] becomes more symmetric relative to the Fermi energy so that the Seebeck coefficient usually decreases monotonically when the doping concentration and Fermi energy increase. For superlattices, however, this product could become more asymmetric because of the step increase of density of states when the Fermi energy moves up and approaches a higher miniband. The resulting nonmonotonic behavior of the cross-plane Seebeck coefficient versus doping was observed experimentally and explained by the miniband formulation and a modified Boltzmann transport model.<sup>18</sup>

However, only the electron wave coupling between two adjacent periods was used to calculate the resonant transmission of electrons and the dispersion curves of minibands were not included in the analysis. Accordingly, the group velocities were not calculated from the dispersion curves and the difference between different minibands could not be considered. As we have discussed, it is necessary to use different group velocities for different minibands because a relatively larger group velocity in a higher miniband is equivalent to the electron energy filtering which can increase the Seebeck coefficient. Furthermore, the strong modification in group velocity has a big impact on the oscillatory behavior of Seebeck coefficient versus doping. In Figure 5, we plot the Seebeck coefficient and the unitless Lorenz number at 300 K using the current model for a short period superlattice structure (well width 6 nm, barrier width 3 nm). Both the Seebeck coefficient and the Lorenz number oscillate with doping concentration.

Although the cross-plane Seebeck coefficient has been analyzed in this paper and previous literatures only for short period superlattices, according to the above discussions we can find that the strong coupling between adjacent wells and in turn a wide miniband formation are not necessary for the nonmonotonic behavior of Seebeck coefficient. In fact, a thicker barrier and the formation of narrow minibands can increase oscillations of the Seebeck coefficient versus doping because the change of density of states with energy is more abrupt in this case. The group velocity of a lower miniband is reduced more than a higher one if the barrier is thicker. This

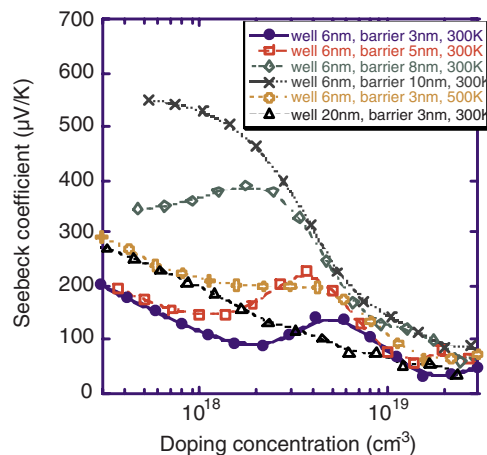


FIG. 6. (Color online) The cross-plane Seebeck coefficient versus doping for several structures with different well thicknesses, barrier thicknesses, and temperatures.

causes the Seebeck coefficient to increase more when the doping increases. However, if the barrier is too thick and the transmission of lower minibands is negligible, the oscillation of Seebeck coefficient with doping can disappear. This is because the conductive higher minibands are more continuous and the density of states changes smoothly with energy. This can be seen in Fig. 6, when the barrier thickness is changed from 3 nm to 5, 8, and 10 nm, respectively. Besides the barrier thickness, there are other factors affecting the oscillatory behavior of the cross-plane Seebeck coefficient. For example, if the temperature increases, the Fermi window  $-\partial f_0/\partial E$  becomes wider and blurs the differential conductivity, which will suppress the oscillation of Seebeck coefficient. This can be seen by the comparison of 300 and 500 K in Fig. 6, while keeping well 6 nm thick and barrier 3 nm thick. Equivalently important, the well thickness determines the spacing of minibands and continuity of density of states. Thicker wells give smaller miniband spacing and suppress the oscillation of cross-plane Seebeck coefficients. This can be seen in Fig. 6 when only the well thickness is changed from 6 to 20 nm.

#### IV. SUMMARY

We investigated the Seebeck coefficient and Lorenz number of superlattices in the cross-plane direction. Charge transfer and band bending were included by a self-consistent solution of coupled Schrödinger and Poisson equations. The thermoelectric properties were then calculated according to the dispersion curves of multiple minibands. The modeling of Seebeck coefficient fits with experimental data very well for a specific superlattice structure at various dopings. In general, the simulation shows that the Seebeck coefficient of superlattices in the cross-plane direction has different temperature dependence compared to bulk materials. The Lorenz number of superlattices in the cross-plane direction can be larger than that predicted by the Wiedemann-Franz law by a factor of 2. In some cases, the superlattice Lorenz number is

reduced by 50%. The oscillation of Seebeck coefficient and Lorenz number with the change of doping concentration is explained using the multiple miniband transport model. A low temperature, a small well thickness, and a moderately thick barrier are favorable to increase the oscillations of cross-plane Seebeck coefficient.

#### ACKNOWLEDGMENTS

This work was supported by the Office of Naval Research through MURI Thermionic Energy Conversion Center program managed by Mihal Gross. Z.B. would like to thank K. Esfarjani and W. Kim for fruitful discussions.

- 
- <sup>1</sup>A. Shakouri and J. E. Bowers, *Appl. Phys. Lett.* **71**, 1234 (1997).  
<sup>2</sup>G. D. Mahan and L. M. Woods, *Phys. Rev. Lett.* **80**, 4016 (1998).  
<sup>3</sup>Z. Bian and A. Shakouri, *Appl. Phys. Lett.* **88**, 012102 (2006).  
<sup>4</sup>D. Vashaee and A. Shakouri, *Phys. Rev. Lett.* **92**, 106103 (2004).  
<sup>5</sup>J. M. O. Zide, D. Vashaee, Z. X. Bian, G. Zeng, J. E. Bowers, A. Shakouri, and A. C. Gossard, *Phys. Rev. B* **74**, 205335 (2006).  
<sup>6</sup>G. Zeng, J. M. O. Zide, W. Kim, J. E. Bowers, A. C. Gossard, Z. Bian, Y. Zhang, A. Shakouri, S. L. Singer, and A. Majumdar, *J. Appl. Phys.* **101**, 034502 (2007).  
<sup>7</sup>R. Venkatasubramanian, E. Siivola, T. Colpitts, and B. O'Quinn, *Nature (London)* **413**, 597 (2001).  
<sup>8</sup>T. C. Harman, P. J. Taylor, M. P. Walsh, and B. E. LaForge, *Science* **297**, 2229 (2002).  
<sup>9</sup>W. Kim, S. Singer, A. Majumdar, D. Vashaee, Z. Bian, A. Shakouri, G. Zeng, J. E. Bowers, J. M. O. Zide, and A. C. Gossard, *Appl. Phys. Lett.* **88**, 242107 (2006).  
<sup>10</sup>M. V. Simkin and G. D. Mahan, *Phys. Rev. Lett.* **84**, 927 (2000).  
<sup>11</sup>R. Venkatasubramanian, *Phys. Rev. B* **61**, 3091 (2000).  
<sup>12</sup>G. Chen, *Phys. Rev. B* **57**, 14958 (1998).  
<sup>13</sup>Y. Chen, D. Li, J. R. Lukes, Z. Ni, and M. Chen, *Phys. Rev. B* **72**, 174302 (2005).  
<sup>14</sup>W. Kim, J. Zide, A. Gossard, D. Klenov, S. Stemmer, A. Shakouri, and A. Majumdar, *Phys. Rev. Lett.* **96**, 045901 (2006).  
<sup>15</sup>D. Vashaee and A. Shakouri, *J. Appl. Phys.* **95**, 1233 (2004).  
<sup>16</sup>L. W. Whitlow and T. Hirano, *J. Appl. Phys.* **78**, 5460 (1995).  
<sup>17</sup>Z. Tao and L. Friedman, *J. Phys. C* **18**, L455 (1985).  
<sup>18</sup>D. Vashaee, Y. Zhang, A. Shakouri, G. Zeng, and Y. J. Chiu, *Phys. Rev. B* **74**, 195315 (2006).  
<sup>19</sup>E. L. Ivchenko and G. E. Pikus, *Superlattices and other Heterostructures* (Springer-Verlag, Berlin, 1997).  
<sup>20</sup>A. M. Cruz Serra and H. Abreu Santos, *J. Appl. Phys.* **70**, 2734 (1991).  
<sup>21</sup>G. S. Nolas, J. Sharp, and H. J. Goldsmid, *Thermoelectrics: Basic Principles and New Materials Developments* (Springer-Verlag, Berlin, 2001).  
<sup>22</sup>M. Lundstrom, *Fundamentals of Carrier Transport* (Cambridge University Press, Cambridge, 2000).